



# Toxins from harmful algal blooms: How copper and iron render chalkophore a predictor of microcystin production

Boling Li<sup>a</sup>, Xiaokai Zhang<sup>b</sup>, Gongjie Wu<sup>c,d</sup>, Boqiang Qin<sup>e</sup>, Boris Tefsen<sup>f,g,\*</sup>, Mona Wells<sup>g,h,\*</sup>

<sup>a</sup> School of Environmental Science and Engineering, Suzhou University of Science and Technology, Suzhou, Jiangsu, 215123, China

<sup>b</sup> Institute of Environmental Processes and Pollution Control, and School of Environmental and Civil Engineering, Jiangnan University, Wuxi, 214122, China

<sup>c</sup> Department of Biochemistry and Systems Biology, University of Liverpool, Brownlow Hill, Liverpool, L69 7ZX, UK

<sup>d</sup> Department of Biological Sciences, Xi'an Jiaotong-Liverpool University, Suzhou, Jiangsu, 215123, China

<sup>e</sup> Taihu Laboratory for Lake Ecosystem Research, State Key Laboratory of Lake Science and Environment, Nanjing Institute of Geography and Limnology, Chinese Academy of Sciences, Nanjing, 210008, China

<sup>f</sup> Microbiology, Department of Biology, Utrecht University, Padualaan 8, 3584 CH, Utrecht, the Netherlands

<sup>g</sup> Ronin Institute, 127 Haddon Place, Montclair, NJ, 07043, USA

<sup>h</sup> Meadows Center for Water and the Environment, Texas State University, San Marcos, Texas, 78666, USA

## ARTICLE INFO

### Keywords:

Eutrophication

Biomolecule regulation

Metal-ligand complexation

Cyanobacterial toxins

Algal assemblage progression

## ABSTRACT

Research on harmful algal blooms has focused on macronutrients, yet recent research increasingly indicates that understanding micronutrient roles is also important in the development of effective environmental management interventions. Here, we report results on metallophore production from mesocosms amended with copper and iron (enzymatic co-factors in photosynthetic electron transport) to probe questions of how cyanobacteria navigate the divide between copper nutrition, copper toxicity, and issues with iron bioavailability. These experiments utilized *Microcystis*, *Chlorella* and *Desmodesmus* spp., in mono- and mixed-cultures in lake water from a large, hypereutrophic lake (Taihu, China). To initiate experiments, copper and iron amendments were added to mesocosms containing algae that had been acclimated to achieve a state of copper and iron limitation. Mesocosms were analyzed over time for a range of analytes including algal growth parameters, algal assemblage progression, copper/iron concentrations and biomolecule production of chalkophore, siderophore and total microcystins. Community Trajectory Analysis and other multivariate methods were used for analysis resulting in our findings: 1) *Microcystis* spp. manage copper/iron requirements through a dynamically phased behavior of chalkophore/siderophore production according to their copper and iron limitation status (chalkophore correlates with Cu concentration,  $R^2 = 0.99$ , and siderophore correlates with the sum of Cu and Fe concentrations,  $R^2 = 0.98$ ). 2) A strong correlation was observed between the production of chalkophore and the cyanobacterial toxin microcystin ( $R^2 = 0.76$ )—Chalkophore is a predictor of microcystin production. 3) Based on our results and literature, we posit that *Microcystis* spp. produces microcystin in response to copper/iron availability to manage photosystem productivity and effect an energy-saving status. Results from this work underscore the importance of micronutrients in influencing harmful algal bloom progression and represents a major advance in understanding the ecological function for the cyanobacterial toxin microcystin as a hallmark of micronutrient limitation stress.

## 1. Introduction

Chalkophores are strong copper (Cu)-binding ligands, i.e., metallophores, that have demonstrated importance in aiding microorganisms to navigate the divide between Cu nutrition and toxicity (Andrei et al., 2020; Badarau and Dennison, 2011). Our previous work is the first we know of that examines chalkophores in natural oxygenated freshwater

environments (Li et al., 2021, and references therein), and in addition to finding that Cu and iron (Fe) micronutrients modulated metallophore production, we also found a microcystin-chalkophore link for *Microcystis* spp. Microcystins, primarily produced by *Microcystis* spp., are the most prevalent cyanobacterial toxins in freshwaters across the world. Despite a vast amount of research focused on the harmful effects of microcystins to humans, animals, and aquatic organisms, the physiological and/or

\* Corresponding authors.

E-mail addresses: [boris.tefsen@ronininstitute.org](mailto:boris.tefsen@ronininstitute.org) (B. Tefsen), [mona.wells@ronininstitute.org](mailto:mona.wells@ronininstitute.org) (M. Wells).

<https://doi.org/10.1016/j.watres.2023.120490>

Received 24 May 2023; Received in revised form 17 July 2023; Accepted 13 August 2023

Available online 14 August 2023

0043-1354/© 2023 The Authors. Published by Elsevier Ltd. This is an open access article under the CC BY license (<http://creativecommons.org/licenses/by/4.0/>).

ecological function of microcystin remains unclear (Omidi et al., 2018; Zhou et al., 2021). The microcystin-chalkophore link is a new clue to aid our understanding of the function of microcystin, particularly as it relates to the effects of micronutrients on bloom-forming algae (Li et al., 2021).

Harmful algal blooms (HABs) have been reported in many lakes around the world, for example, Lake Erie (USA), Lake Winnipeg (Canada), and Taihu (太湖 in Chinese, i.e., Lake Tai, China; Ulrich et al., 2016; Watson et al., 2016; Qin et al., 2019), and thus HABs have been described as the greatest inland water quality threat inasmuch as HABs cause multiple ecological problems (Brooks et al., 2016; Paerl, 2018; Zhou et al., 2021). Eutrophication from excess anthropogenic nitrogen (N) and phosphorous (P) is a major cause of HABs (Paerl et al., 2011; Quiblier et al., 2013; Gobler et al., 2016) and, along with climate change, a driver of increased HAB prevalence (Paerl and Huisman, 2008; Gobler, 2020). A wide range of algal cellular processes additionally require micronutrients (nine micronutrients discussed in Andersen's Definitive Text, 2005). The role of micronutrients in influencing HAB progression is much less studied and at the same time increasingly recognized because relatively small changes in micronutrient status have wide-ranging consequences (Facey et al., 2019; Zhang et al., 2019).

Cu and Fe are notably essential for algal growth because they are required as enzymatic co-factors in photosynthetic electron transport (Quigg, 2008, 2016). Cyanobacteria and a number of eukaryotic green algae possess two distinctive electron carriers, one Cu-based, the other Fe-based, which facilitates the nutritional flexibility of these organisms given that the bioavailability of environmental Fe is often low (Ho and Krogmann, 1984; Merchant and Bogorad, 1986). For *Microcystis* spp., electron transport between Photosystems I (PSI) and II (PSII) is achieved by *c*-type cytochrome (Cyt<sub>c</sub>) or plastocyanin (PC), respectively bound to Fe or Cu as a co-factor (Ho and Krogmann, 1984). Availability of these essential metals is long known to determine which system is used in electron transport (Sandmann and Böger, 1980). Recent research reveals that cyanobacterial PC- and Cyt<sub>c</sub>-encoding genes are regulated by Cu at the transcriptional level (García-Cañas et al., 2021), the manner of which Blaby-Haas (2021) comments upon as "suggesting that replacement of PC with Cyt<sub>c</sub> may involve posttranslational adjustment of some photosynthetic complexes, hinting at potentially uncharted complexity".

The Cu/Fe switching ability in the photosynthetic electron transport system relates to differential bioavailability of Cu/Fe. Chalkophores and siderophores (strong Fe-binding ligands) have demonstrated importance in aiding organisms to manage environmental Cu and Fe bioavailability (Saha et al., 2016; Solioz, 2018). Some algal siderophores are themselves copper complexes, i.e., the siderophore molecule itself is an organometallic complex that contains Cu, and some siderophores of this type have been reported to assist with Fe acquisition, resulting in a synergistic growth response when both Cu and Fe are added to growth media of Fe-stressed cells (Peers et al., 2005). This is consistent with a model wherein, at low Fe, Cu simultaneously is associated with improved Fe uptake and increased Cu internalization (Schoffman et al., 2016; Kochoni et al., 2022). In some cases, Cu and Fe share the same cellular uptake systems (Zhen et al., 2021). While algal growth is promoted when the concentration of Cu is low enough to be nontoxic (Manahan and Smith, 1973; Zhang et al., 2019), there is a Cu/Fe interplay at toxic Cu concentrations as well, with one recent study having shown that increased Fe reduced Cu toxicity for the green algae *Chlamydomonas reinhardtii* (Kochoni and Fortin, 2019). Nicolaisen et al. (2010) reported that the cyanobacteria *Anabaena* spp. increase production of the siderophore schizokinen at high Cu to achieve Cu detoxification. Clearly a better understanding of biomolecular controls of Cu and Fe bioavailability is needed.

Concerning microcystin production, one hypothesis has been that microcystin serves as a siderophore (Martin-Luna et al. 2006a), that is, it helps manage cellular Fe and/or Fe acquisition. In our previous work we found no apparent microcystin-siderophore link, and others have pointed out that, functionally (in terms of binding strength), microcystin

is not a siderophore. Because microcystin is not a siderophore, we did not expect a metallophore link and were therefore surprised by our unexpected discovery of a hitherto unreported microcystin-chalkophore link (Li et al., 2021). In view of the relative paucity of research concerning micronutrient effects on blooms, metallophore and microcystin production, here we report results from small-scale mesocosm studies of how *Microcystis* spp. and green algae metallophore and microcystin production changes with different Cu and Fe amendments.

## 2. Materials and methods

### 2.1. Study design

In nutrient limitation bioassays (NLBs), we previously observed modulated production of chalkophore and siderophore in response to Cu/Fe amendments and a previously unreported link between chalkophore and microcystin production. Our purpose here is to investigate this further while 1) varying the level of Cu in amendments and 2) increasing the level of algal Cu and Fe limitation at the outset of experiments.<sup>1</sup>

The NLB experiments included three types of mesocosm to see if micronutrient effects differ for *Microcystis* spp., as compared to green algae, and a mixture of these two. *Microcystis* spp. were selected for HAB-mesocosms ( $M_{\text{meso}}$ ) because these algae are the main HAB-forming species in our field site and a major source of HABs worldwide (Harke et al., 2016; Qin et al., 2019; Kruk et al., 2021). *Microcystis* spp. are also well-studied because they produce the microcystin toxin, for reasons not yet clear (Omidi et al., 2018). *Desmodesmus* and *Chlorella* spp. were selected for contrasting, non- nuisance green algae mesocosms ( $G_{\text{meso}}$ ). We also added mesocosms with a 1:1 mixture of  $M_{\text{meso}}$  and  $G_{\text{meso}}$  ("both" components,  $B_{\text{meso}}$ ), which is more reflective of competition between the cyanobacteria/green algae in natural settings (Zhang et al., 2019; Li et al., 2021). For more detail on algae selection and Cu/Fe sensitivity, see the Supplementary Material (SM). Our field site is Lake Taihu, and we used water from Taihu's Xukou Bay in mesocosms as we have found that micronutrient mesocosm responses reflect geographic differences in lake water chemistry, and the strongest effects for micronutrient amendment were for mesocosms using water from this site (Zhang et al., 2019; Li et al., 2021).

We varied the level of Cu to observe Cu influences as a nutrient or as toxicant. We included Fe in some amendments to investigate Cu/Fe interactive influences on algal growth, including whether Cu and Fe synergistically affect growth (per the discussions in Schoffman et al., 2016; Zhen et al., 2021; Kochoni et al., 2022, and in the Introduction above) and whether Fe reduces Cu toxicity (Nicolaisen et al., 2010; Kochoni and Fortin, 2019). For all amendments, we were interested to observe differences in chalkophore/siderophore/microcystin production under conditions wherein algae were even more Cu/Fe limited than our previous work. With our hitherto unreported discovery of a microcystin-chalkophore link, we were greatly interested to see if we would again observe this link, how the relationship might vary with different levels of Cu amended, and how this might or might not relate to Cu-/Fe-limitation.

Based on the foregoing considerations, we designed the micronutrient-dosing scheme to include 1) Control (Ctl), no micronutrient added, 2) CuLo, where the level of Cu added was targeted to be nontoxic (low), with the possible influence of Fe-limitation, 3) CuLo-FeHi, with "high" Fe (a designation indicating comparative concentration to the initial water quality, Table S1, as defined by Xu et al., 2013), as a contrast to CuLo, 4) CuHiFeHi targeted to have a Cu concentration high enough to have an inhibitory/toxic effect on *Microcystis*, while also

<sup>1</sup> For a detailed discussion of the use of this approach for large factorial experiments, including those that screen for environmental micronutrient effects, see Zhang et al., 2019; Li et al., 2021 and references therein.

being low enough to have no or a less inhibitory effect on green algae, providing a possible opportunity for green algae to outcompete *Microcystis* (e.g., in  $B_{\text{meso}}$ ) and to see if the high Fe would ameliorate Cu toxicity. Table 1 lists details for the four amendments used for NLBs in this work. For a detailed discussion concerning how these concentrations were chosen, see the SM.

## 2.2. Field site and preparation of water and algae for nutrient limitation bioassays

Taihu, China's third largest freshwater lake (2,338 km<sup>2</sup> surface area; catchment area 36,900 km<sup>2</sup>), is polymictic, hypereutrophic, and an important drinking water source for at least 11 million people (Qin et al., 2007; Xu et al., 2017). As a result of development in the Yangtze Delta region around Taihu, cyanobacterial HABs and microcystin pollution occur in Taihu every summer since the mid-1980s (Wang et al., 2009; Qin et al., 2019; Xue et al., 2020), such that Taihu is an important field site for research on HAB management (Qin et al., 2019). Fig. 1 is a map of Taihu showing locations pertinent to work here, including 1) our water collection site, Station 28, in Xukou Bay, where station signifies a quarterly monitoring site of the Nanjing Institute of Geography and Limnology (NIGLAS), Chinese Academy of Sciences, 2) the *Microcystis* collection site (immediately offshore from the Lujiangkou Algal-water Separation Facility) in Meiliang Bay (Station 6), and 3) the site of mesocosm experiments, Taihu Laboratory for Lake Ecosystem Research (TLER). For researchers employing the approach we do here, it is desirable to use algae from Taihu, however, the goal is to use effectively pure cultures for *Microcystis* spp., which only occur during strong HABs. Therefore, the collection site varies, and must be chosen where the *Microcystis* bloom has verifiably reduced occurrence of all other algal species to effectively nil (Xu et al., 2013; Li et al., 2021). The approach used here has been used by our group and others and is accepted practice for reasons outlined in literature (Millican et al., 2008; Li et al., 2021; Frost et al., 2023).

Forty-L of water was collected at Station 28 in Xukou Bay from 0.2 m below the surface into an acid-cleaned polyethylene carboy. Field measurements included water temperature, turbidity and pH, measured using a YSI 6600 sonde. The water sample was filtered immediately after collection to remove *in situ* phytoplankton using Whatman GF/F glass-fiber filters, nominal pore size 0.7  $\mu\text{m}$ . When filtering such a large volume as 40-L, many filters must be used due to filter clogging. During the many filter changes needed, minute amounts of algae from the used filter cake transfer to the filter housing, hence filtrate. The *in situ* algae transfer is confirmed to be below the limit of detection by microscopic counting (this study, also see more detailed commentary in Li et al., 2021). Over the time course of our experiments, the *in situ* algae may increase in mesocosms; we do not take more stringent steps to avoid this since the ability for the algal assemblages to shift is more reflective of natural field conditions. The process of filtering the water removes *in situ* algae sufficiently to ensure that the initial assemblages are the HAB-forming *Microcystis* and non-nuisance green algae (Li et al., 2021).

The *Microcystis* collection site, Station 6, is immediately offshore

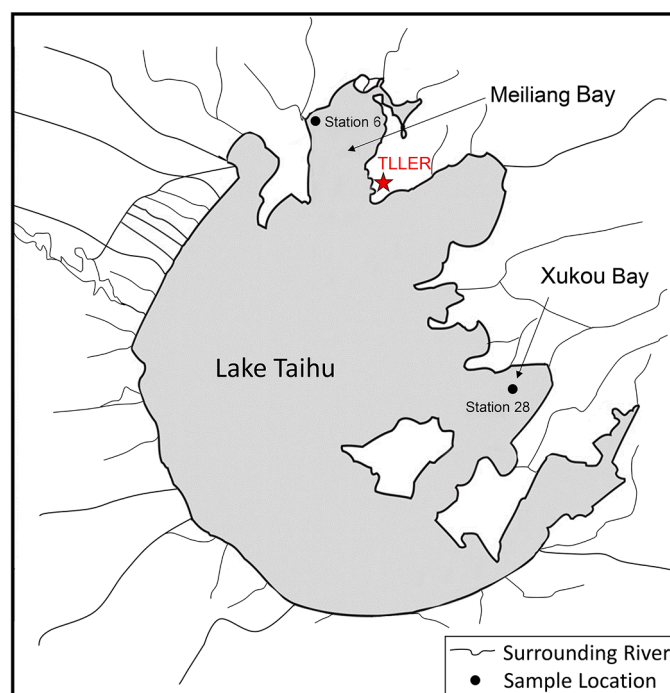


Fig. 1. Map of Taihu showing Station 6 (Lujiangkou Algal-water Separation Facility in Meiliang Bay, site for collection of *Microcystis*), Station 28 (in Xukou Bay, water collection site), and the Taihu Laboratory for Lake Ecosystem Research (TLER, the site where mesocosm experiments were performed).

from the Lujiangkou Algal-water Separation Facility, where the predominant current and wind conditions in Taihu dependably transport and concentrate HAB-algae. The now longstanding history of extreme HAB development in Taihu every summer has necessitated construction of this purpose-built facility to remove HAB-algae from Taihu water. This location is ideal for collecting the exact *Microcystis* consortia comprising Taihu HABs. *Microcystis* were collected at Station 6 in Meiliang Bay after the onset of a HAB and verified to be > 99% *Microcystis* spp. from microscopic examination. *Desmodesmus* and *Chlorella* spp. were purchased from Aquatic Biology Services (Wuxi Zhongshun Biotechnology Co., Ltd) and confirmed to be > 99% *Desmodesmus* and *Chlorella* from microscopic examination. Subsequent to acquisition, algae were immediately subject to acclimation for micronutrient depletion and to withstand the harsh environment of Taihu. Acclimation continued up until NLB experiments, and immediately prior to mesocosm dosing, algae were collected/concentrated by coarse filtration (Li et al., 2021). See SM for more details on algal acclimation.

## 2.3. Nutrient limitation bioassays

To initiate NLBs, filtered Station 28 lake water was divided into three portions and dosed to reach an initial optical density at 750 nm of  $\sim 0.05$  ( $OD_{750}$ , hereafter OD, the wavelength recommended by Griffiths et al., 2011) to avoid spectral interference from algal pigments) using concentrated algal cultures of 1) *Microcystis* spp. ( $M_{\text{meso}}$ ), 2) a 1:1 mixture of OD  $\sim 0.05$  *Desmodesmus* and *Chlorella* spp. ( $G_{\text{meso}}$ ), and 3) half the amount of each algae used to dose  $M_{\text{meso}}$  and  $G_{\text{meso}}$  ( $B_{\text{meso}}$ , 1:1  $M_{\text{meso}}:G_{\text{meso}}$ ). After dosing water with acclimated algae, triplicate subsamples were placed into 1-L chemically inert, transparent mesocosm cubitainers for each NLB permutation and spiked to achieve the final concentrations of amendments. All work was conducted using ultrapure water and under trace-metal clean conditions. Immediately after dosing water with algae and spiking with amendments as listed in Table 1 above, the cubitainers were incubated *in situ* at TLLER (Fig. 1). Initial water and algal suspensions ( $t_0$ ) were sampled for analysis at the time of NLB deployment.

Table 1  
Amendment schedule used in Taihu NLB experiments.

	N <sup>a</sup>	P <sup>b</sup>	Cu <sup>c</sup>	Fe <sup>d</sup>
Control	2.0 mg·L <sup>-1</sup> N	0.2 mg·L <sup>-1</sup> P	No added Cu	No added Fe
CuLo	2.0 mg·L <sup>-1</sup> N	0.2 mg·L <sup>-1</sup> P	20 $\mu\text{g}\cdot\text{L}^{-1}$ Cu	No added Fe
CuLoFeHi	2.0 mg·L <sup>-1</sup> N	0.2 mg·L <sup>-1</sup> P	20 $\mu\text{g}\cdot\text{L}^{-1}$ Cu	200 $\mu\text{g}\cdot\text{L}^{-1}$ Fe
CuHiFeHi	2.0 mg·L <sup>-1</sup> N	0.2 mg·L <sup>-1</sup> P	100 $\mu\text{g}\cdot\text{L}^{-1}$ Cu	200 $\mu\text{g}\cdot\text{L}^{-1}$ Fe

<sup>a</sup> Added as KNO<sub>3</sub>.

<sup>b</sup> Added as K<sub>2</sub>HPO<sub>3</sub>·3H<sub>2</sub>O.

<sup>c</sup> Added as CuSO<sub>4</sub>·5H<sub>2</sub>O.

<sup>d</sup> Added as FeCl<sub>3</sub>·6H<sub>2</sub>O (a less bioavailable form of Fe, see detailed discussion in SM).



Each cubitainer was subsequently sampled another four times for analysis, at days 2, 4, 6 and 8 (t2, t4, t6 and t8).

## 2.4. Sample and data analysis

Mesocosm subsamples were analyzed for a range of analytes as a matter of routine (e.g., Zhang et al., 2019; Li et al., 2021). The relevant determinands discussed here include OD, algal identification and counts (microscopic, Cts.m), total metals (TM, includes total Cu, TCu, and total Fe, TFe), total dissolved metals (TDM, including TDCu and TDFe), chalkophore, siderophore and microcystins. See SM for details on measurement methods for determinands. For data analysis using multi-pairwise comparison, Tukey's Honest Significant Difference (HSD)  $Q_{\text{sample}}$  was calculated and compared with values of  $Q_{\text{crit}}$  obtained from Gleason's Q-value table (Gleason, 1999; Li et al., 2021). The criterion of  $p < 0.05$  was used for rejection of  $H_0$ ; individual  $p$ -values were calculated using Lane's  $p$ -value calculator (Lane, 2015).

Community Trajectory Analysis has been recently adduced as a fresh perspective on dynamic aspects of population/community changes, including time series biomolecule production by algae (De Cáceres et al., 2019; Li et al., 2021). Here we additionally employ trajectory analysis techniques calculating multivariate trajectory distances (McCune and Grace, 2002) and time-lagged cross correlation of trajectories (Kushkevych and Beno, 2013). The dynamic time warping (DTW) approach as a distance metric was used for multivariate trajectory analysis (Bar-Joseph et al., 2003; Yuan et al., 2011; Cleasby et al., 2019). In order to conduct the time-lagged cross correlation, resampling or sample-rate conversion (upsampling and downsampling) is needed to reformat discretization for the biological time-series data (Oppenheim et al., 1999; Sundararajan, 2021). The smacof, vegclust, SimilarityMeasures, caret, stats, graphics, and grid packages in R were used to perform the calculations needed for Community Trajectory Analysis, time-lagged cross correlation and DTW calculations (de Leeuw and Mair, 2009; De Cáceres et al., 2010; Max, 2021; R Core Team, 2021). See SM for additional details.

## 3. Results and discussion

### 3.1. Cu/Fe-induced changes in mesocosm assemblages

The pie charts in Fig. 2 show temporal changes in algal assemblages in response to amendment for different groups of algae. We previously found a strong correlation between OD and Cts.m, however, with substantial scatter around the trend (Li et al., 2021). Here, we again see a significant OD-Cts.m correlation (see SM for pairwise-correlations of all inter parameter associations). While Cts.m and OD both reflect growth, OD is a bulk solution measurement that reflects how cells in solution reduce transmission of light (related to volume); Cts.m does not distinguish cell size/volume, however, remains the dependable standard for simple determination of number of algae, assemblage changes and cell condition (Butterwick et al., 1982; Li et al., 2021). We focus on OD here. The pie charts in Fig. 2 show temporal changes in algal assemblages in response to amendment for different groups of algae, with pie-chart diameter/sizes varying in proportion to OD (for interested readers, univariate plots of OD versus time can be found in SM). The five algal groups, per Li et al., 2021, were designated as 1) Blue-green, BG—97+% *Microcystis* with smaller amounts of *Chroococcus* and *Pseudoanabaena*, 2) Desmids (Des)—*Desmodesmus*, with occasional occurrences of *Scenedesmus*, 3) Unicellular green algae (UG)—mixtures of *Carteria* and *Chlorella*, with lesser amounts of *Chlamydomonas*, 4) Diatoms (Dia)—mixtures of *Navicula* and *Nitzschia*, with minor amounts of *Asterionella*, *Cyclotella*, and *Fragilaria*; and 5) the Rest—comprised of low, highly variable, counts of other species not included above. Algal assemblage transitions favoring either blue-green or green algae as a function of varying NP/carbon is well-known (Shapiro, 1973); it is a relatively recent discovery that micronutrients are strong mediators of algal assemblage changes (Zhang et al., 2019; Li et al., 2021).

Fig. 2 to Cts.m and OD are as expected. For  $M_{\text{meso}}$ , algae are 100% BG (specifically *Microcystis* spp.). We were reasonably satisfied that the  $G_{\text{meso}}$  t0 Cts.m ratio of 41% Des: 59% UG was close to 50:50, since the  $G_{\text{meso}}$  Des/UG mixture was effected using OD, whereby Des constitute larger, but fewer, individuals, while UG in  $G_{\text{meso}}$  constitute smaller, but more numerous, individuals. Similar comments pertain to  $B_{\text{meso}}$  given the relatively small size of *Microcystis* cells.

For  $M_{\text{meso}}$ , the overall trend of growth only occurs for Cu-containing

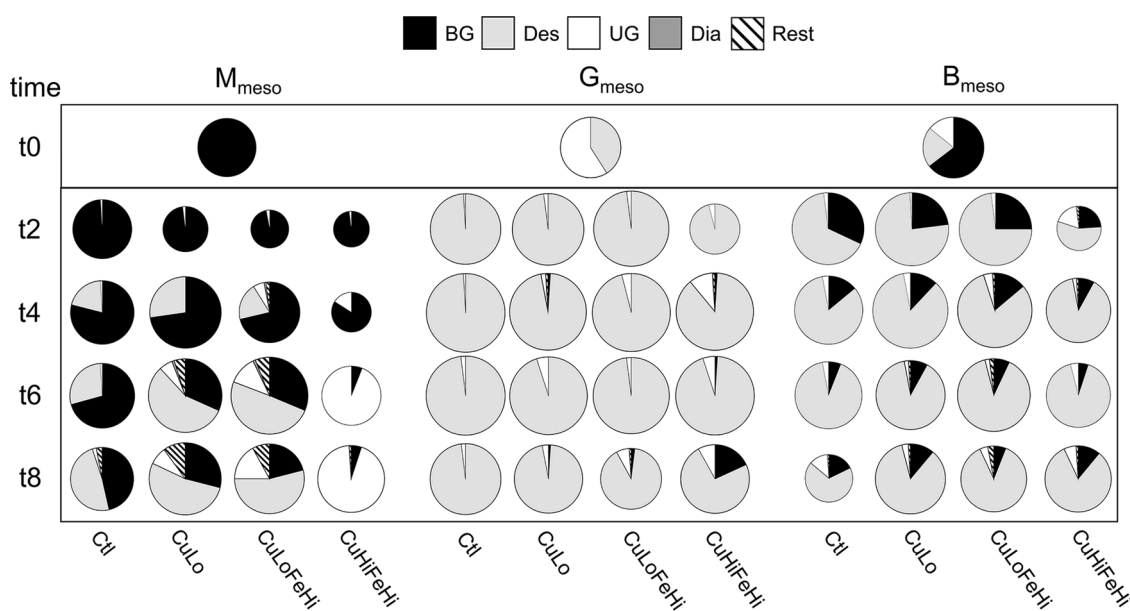


Fig. 2. Pie charts showing changing proportions of algal Cts.m for different amendments; pie charts vary in size in proportion to OD (at 750 nm) for each sample (the OD ranged from a minimum of 0.02 to a maximum of 0.08. Abbreviations are BG = Blue-green algae; Des = Desmids; UG = Unicellular green algae; Dia = Diatoms; Rest = remaining, less common algae).

amendments after a sharp drop in OD by t2. After t2 there are similar notable changes in  $M_{\text{meso}}$  assemblages. Other than CuHiFeHi,  $M_{\text{meso}}$  Des increases t4–t8 to become the dominant species by t8, however, the process occurs more slowly for Ctl, and is similar for CuLo compared with CuLoFeHi. By t8, 46%, 29% and 21%, respectively, of BG remain in  $M_{\text{meso}}$  Ctl, CuLo and CuLoFeHi. That Des slowly took over  $M_{\text{meso}}$  Ctl over t0–t8 suggests that Cu amendment alone is not responsible for the change. In terms of absolute Cts.m, *Microcystis* increases to a maximum (versus t0) at t2 in the Ctl (191%) and t4 in CuLo (159%). We note that while the Cts.m for *Microcystis* spp. in Ctl has increased greatly by t2, cells appear to be considerably smaller, consistent with the concomitant relatively low t0–t2 increase in OD. In contrast to Ctl and CuLo, for CuLoFeHi, *Microcystis* Cts.m show a small decrease of 10% by t4, compared to t0 (accompanied by a small but monotonic OD increase), with a sharper decrease thereafter. The  $M_{\text{meso}}$  Ctl OD had a maximum increase of 24% by t6 at the onset of stationary phase, and by t8, at 46% *Microcystis* spp., green algae could not be said to have dominated. Interestingly, Fe is consistently associated with a larger t2 OD decrease. OD for CuLoFeHi decreases by 58% and OD for CuHiFeHi decreases by 61%, whereas OD for CuLo only decreases by 40% at t2. The initial OD drops for metals-amended mesocosms were similar (~20%); the  $M_{\text{meso}}$  OD recovery for CuLo, CuLoFeHi and CuHiFeHi from t2–t8 followed the order CuLo > CuLoFeHi > CuHiFeHi, with the former two reaching stationary phase by the end of the experiment, whereas CuHiFeHi did not.

Assemblage changes for  $M_{\text{meso}}$  CuHiFeHi were much larger and different, with only 4.8% *Microcystis* left at t8. A striking feature in Fig. 2 is that by t4 UG began to replace BG/*Microcystis*, continuing through to t8. This replacement of *Microcystis* by UG for the high Cu is consistent with our previous results (Zhang et al., 2019; Li et al., 2021). The percentage of UG in  $M_{\text{meso}}$ , on average, follows CuHiFeHi > CuLoFeHi > CuLo > Ctl over time, with only 2% UG in  $M_{\text{meso}}$  Ctl by t8. The replacement of BG/*Microcystis* by UG is strongly associated with Cu, and secondarily with Fe since UG in CuLoFeHi > CuLo. Phenomenologically, this finding is consistent with other works indicating that some UG species are relatively more tolerant to and/or requiring Cu (Bilgrami and Kumar, 1997; Merchant, 1998; Zhang et al., 2019); however, more work is needed to understand the mechanistic basis.

For  $G_{\text{meso}}$ , the rapid dominance by Des is the only large assemblage change and is not amendment specific. All  $G_{\text{meso}}$  ODs reflect a similar trend of growth (a maximum of 166% at t6 compared to t0). There were no statistically significant differences except for CuHiFeHi, which had significantly lower OD than all other amendments at t2. The decrease in OD for CuHiFeHi from t0–t2 is a result of a near total elimination of UG (t2 Cts.m were 0.06% of t0) and a relatively slower rate of increase in Des (41% that of the average Des increase in other mesocosms). The minor assemblage component of UG is somewhat more persistent for all amendments (averaging 4.5% over t2–t8), as compared to Ctl (an average UG of 1.6% over t2–t8). We did not see large  $G_{\text{meso}}$  UG differences with amendment as we saw for  $M_{\text{meso}}$ , however, there is still an order, following CuHiFeHi (7%) > CuLo ~ CuLoFeHi (3%) > Ctl (2%). The only other point to note for  $G_{\text{meso}}$  is the t8 increase of BG to 18% for CuHiFeHi, by which time all cultures were post-stationary (average OD 25% lower than at t6). This BG count was almost completely comprised of *Pseudonabaena*, not *Microcystis* spp.

The  $B_{\text{meso}}$  share commonalities with both  $M_{\text{meso}}$  and  $G_{\text{meso}}$ . Like  $M_{\text{meso}}$ , the persistence of BG/*Microcystis* was highest in Ctl, similar for CuLo/CuLoFeHi (84/88% of Ctl by Cts.m) and lowest for CuHiFeHi (41% of Ctl Cts.m). As with  $G_{\text{meso}}$ , Des rapidly displace UG by t2; the percentage of Des increases from 21%, at t0, to 66%, 76%, 73%, and 56% by t2 for Ctl, CuLo, CuLoFeHi, and CuHiFeHi, respectively, with the majority of the remainder in all cases being *Microcystis* spp. The average t2–t8 UG in  $B_{\text{meso}}$  was higher for CuHiFeHi, though not statistically significant. The  $B_{\text{meso}}$  transition of algal assemblages compared to  $M_{\text{meso}}$  and  $G_{\text{meso}}$ , showed an apparent resurgence of UG in the Ctl by t8. From OD results, the culture is crashing by t8, and the UG was constituted of

an equal amount of *Carteria* (47%) and *Chlamydomonas* (53%), i.e., not the *Chlorella* that was present at t0. The OD behavior over time for  $B_{\text{meso}}$  is similar as for  $G_{\text{meso}}$ , except that a relatively flat OD at stationary phase persists to t8 for all mesocosms save Ctl.

All mesocosms were affected by the high Cu; in Fig. 2, the OD decreases t0–t2, are, respectively, 61%, 32%, and 48% for  $M_{\text{meso}}$ ,  $G_{\text{meso}}$ , and  $B_{\text{meso}}$ , with the drop in OD for  $G_{\text{meso}}$  being half that of  $M_{\text{meso}}$ . The OD decrease for  $B_{\text{meso}}$  averages that of  $M_{\text{meso}}$  and  $G_{\text{meso}}$ . Though the high Cu decreased the growth of green algae by t2, the OD recovery was quicker for green algae in  $G_{\text{meso}}$  compared to *Microcystis* in  $M_{\text{meso}}$ . That the trend of the OD change with time is similar for  $G_{\text{meso}}$  and  $B_{\text{meso}}$  is explainable from microscopic examination wherein we found that the percentage of BG/*Microcystis* in  $B_{\text{meso}}$  was overtaken by green algae during the course of the experiment.

A question that immediately arises for us regarding Fig. 2 results is to what extent bioavailable Cu/Fe changes with assemblages/OD. On cursory examination of TDM, we find that both TDCu and TDFe do vary over time (see SM), however not in a way obviously relating to patterns in Fig. 2. Both TDCu and TDFe appear to undergo exponential decrease to steady-state by t2, consistent with sorption behavior, although an additional decrease is seen for TDCu in  $M_{\text{meso}}$  by t8 associated with ingrowth of green algae. For TDCu, t2 *Microcystis*/ $M_{\text{meso}}$  uptake is ~40% that of green algae/ $G_{\text{meso}}$ , in agreement with our previous findings (Li et al., 2021) and literature reports (see SM). In the case of TDFe, results are similar for all mesocosms. The decrease in TDFe by t2 could result from sorption or formation of insoluble species such as Fe-oxyhydroxides. The latter is quite likely based on the  $\text{Fe}^{3+}$  form used in amendments and well-known chemical equilibria governing iron oxyhydroxide formation. The values of TDFe that we observe, however, are well above what chemical equilibria would allow. This suggests that some TDFe has formed colloids that pass through the filter (operational standard for TDM). Details concerning quality analysis/quality control for TM/TDM analysis and results, as well as results from analysis for Station 28 initial water quality (Table S1), are given in the SM.

### 3.2. Results from community trajectory analysis of chalkophores and siderophores

Selected Community Trajectory Analysis for chalkophore and siderophore production as a function of Cu/Fe amended are shown in Fig. 3 (see Fig. S4 in the SM, for raw data versus time). There are distinct patterns resulting from amendments. The changes in chalkophore in  $M_{\text{meso}}$  are inversely proportional to TCu amended (Fig. 3A); though only averages for each amendment are shown in each panel for Fig. 3, the averages are based on 12 independent mesocosm experiments for each mesocosm type. The  $p$ -values and  $R^2$  values shown are based on the independent experiments, and the strong correlations shown correspond to a high level of statistical significance. Chalkophore in t0  $M_{\text{meso}}$  was 2.9  $\mu\text{eq}$  EDTA/L (equivalents ethylene diamine tetra-acetic acid, see SM), and the maximum level was 6.1  $\mu\text{eq}$  EDTA/L at t4. The only decrease in chalkophore production was for CuHiFeHi, most marked by t2. This may relate in part to the decrease of *Microcystis* by t2, however, the decrease in chalkophore production (83%), is substantially greater than the t0–t2 decrease in OD (62%) or *Microcystis* Cts.m (31%). Fig. 3B slopes for  $G_{\text{meso}}$  chalkophore versus TCu are not differentiable from zero; CuLo chalkophore is lower than that for CuLoFeHi at t2 ( $p < 0.05$ ). This is quite different than for  $M_{\text{meso}}$ , with additional differences being that  $G_{\text{meso}}$  t0 chalkophore was zero, with the maximum chalkophore production being around half that of  $M_{\text{meso}}$  (52%).  $B_{\text{meso}}$  t0 chalkophore was the average of that of  $M_{\text{meso}}$  and  $G_{\text{meso}}$  to within statistical uncertainty, then following the behavior of  $G_{\text{meso}}$  chalkophore production (Fig. S3C);  $B_{\text{meso}}$  had higher chalkophore than  $G_{\text{meso}}$  in all cases by t8, presumably because of the persistence of some *Microcystis* by that time (Fig. 2). The overall trends in Fig. 3A–C are the same on an OD-normalized basis (ordinate axis), albeit with lower correlations (see SM).

While chalkophore production inversely proportional to TCu is a

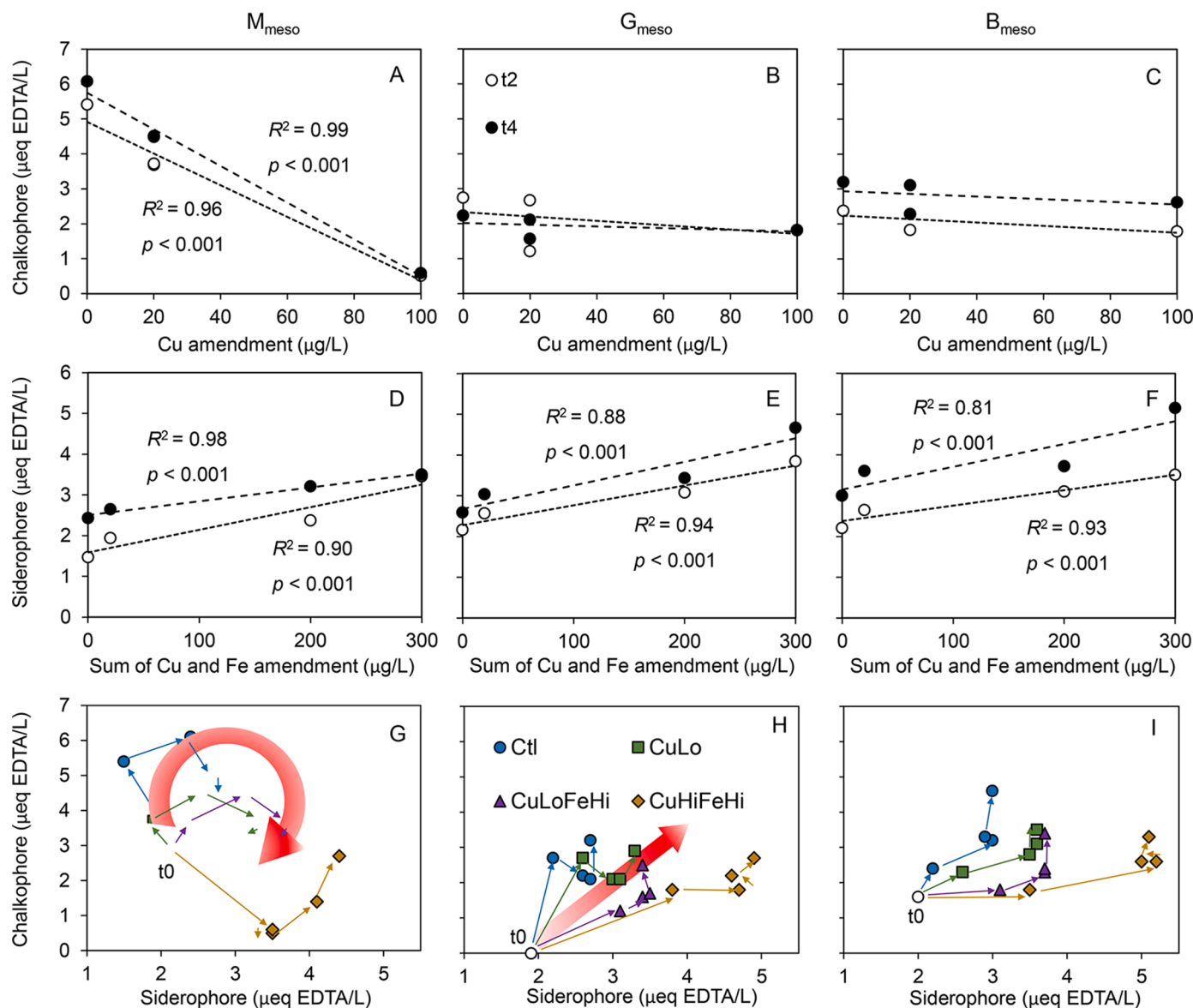


**Fig. 3.** Chalkophore/siderophore correlations with the amount of metal amended and chalkophore/siderophore bivariate community trajectories. Chalkophore/siderophore are reported as  $\mu\text{eq EDTA}$  (Li et al., 2021). Results are plotted as a function of mesocosm type for chalkophore correlations with Cu amended (A–C), siderophore correlations with the sum of Cu and Fe amended (D–F), and chalkophore/siderophore bivariate community trajectories (G–I). Each line in panels A–F represents results from 12 independent experiments comprised of four amendments, each of which in turn includes three independent replicates. For visual clarity, results from each of the three replicates are averaged, however, the  $p$ -values and  $R^2$  values shown are based on the twelve independent experiments. For the strong correlations in panels A, D, E, and F, the  $p$ -values correspond to a high level of statistical significance.

characteristic of  $M_{meso}$  (Fig. 3A–C), changes in siderophore were quite different. In Fig. 3D–F, the pattern for siderophore production is the same across mesocosms and is directly proportional to the sum of TCu and TFe amended (correlations shown statistically significant as compared to TFe alone). Such correlation only persists on an OD-normalized basis for  $M_{meso}$  (see OD-normalized results in SM). Despite the relative bioavailability of Fe given the form in which we amended it, when Fe is present, siderophore production is modulated in response (Li et al., 2021). In fact, the non-cognate metal Cu seems to stimulate siderophore production as well as Fe, in keeping with others' findings of strong siderophores binding to Cu (McKnight and Morel, 1980; Nair et al., 2007; Holden and Bachman, 2015) and that Cu/Fe share cellular uptake systems (Kochoni et al., 2022). The trends of chalkophore and siderophore production in micronutrient-limited mesocosms are all suggestive of a rapid response to the influx of initially highly bioavailable metal as amended, despite the rapid diminution of TDM (Fig. S3).

Turning now to the Community Trajectory Analysis, in general, the trajectories (Fig. 3G–I) of chalkophore/siderophore for  $M_{meso}$  in Fig. 3 are very different than for  $G_{meso}$  and  $B_{meso}$ . There is an evolution of the trajectories for all mesocosms, from one spatial behavior (Ctl) to another through the progression CuLo, CuLoFeHi, to CuHiFeHi. For  $M_{meso}$ , chalkophore/siderophore showed circular trajectories, clockwise for Ctl, CuLo and CuLoFeHi and counter-clockwise for CuHiFeHi. The behavior for  $M_{meso}$  (wide red arc) reflects an adaptive strategy, whereby there are preferential changes according to whether Cu or Cu-and-Fe is present. When amended with high Cu, the trajectory direction for  $M_{meso}$  changed due to the immediate decrease/cessation of  $t_0$ – $t_2$  chalkophore production. When comparing  $M_{meso}$  Ctl with CuLo and CuLoFeHi, a differential chalkophore increase from  $t_0$ – $t_2$  resulted in a higher initial trajectory along the chalkophore/y-axis. In fact, for the Ctl, and to a lesser extent CuLo, the only other amendment without Fe, the initial chalkophore production is accompanied by a decrease in siderophore; siderophore

production only begins as chalkophore production tapers. In contrast, there is no decrease of t0–t2 siderophore for Fe-amended mesocosms, which exhibit longer trajectories on the siderophore/x-axis.

The  $G_{\text{meso}}$  trajectories are much different than those for  $M_{\text{meso}}$ . Rather than being described in terms of rotation, they could all be approximated in polar coordinates as vectors, the angle and magnitude of which varies relative to the amounts of t0 Cu or Fe (e.g., wide red arrow). While we describe  $M_{\text{meso}}$  as adaptive, changing chalkophore/siderophore differentially, in contrast  $G_{\text{meso}}$  chalkophore/siderophore trajectories could be approximated as vectors in polar coordinates because levels changed simultaneously. For  $G_{\text{meso}}$ , the trajectories for all mesocosms start from  $y = 0$  due to absence of detectable t0 chalkophores. The major differences in trajectories for  $G_{\text{meso}}$  correspond to changes resulting in shorter or longer trajectories on the siderophore/x-axis.

For  $B_{\text{meso}}$ , even t0–t2 when there is still an appreciable amount of *Microcystis* present, we do not see the rotation-type trajectory shape that we see for  $M_{\text{meso}}$ . When amended with Cu and having a lower amount of *Microcystis* relative to the Ctl,  $B_{\text{meso}}$  trajectories become more similar to those of  $G_{\text{meso}}$ , consistent with the changes in algal assemblages.  $B_{\text{meso}}$  chalkophore increases are most pronounced when greater quantities of *Microcystis* are present, which may relate to the interesting microcystin-chalkophore link discussed in our previous work (Li et al., 2021) and further below. For  $G_{\text{meso}}$  and  $B_{\text{meso}}$ , siderophore is for the most part increasing (longer x-axis trajectories), with no substantive decrease at any point. The trajectory view of chalkophore/siderophore interactions, is, to our thinking, a more informative way to consider the inter-relationship between the two.

The DTW technique was used to analyze trajectory similarities, and results are shown in Fig. 4. From DTW analysis, trajectories for all amendments are significantly different from each other ( $p < 0.05$ , Tukey's HSD). We find that, no matter how we analyze the data (see SM for different trajectory formulations), CuHiFeHi is always most different from all other trajectories. For  $M_{\text{meso}}$  and  $B_{\text{meso}}$  the greatest similarities/smallest DTW distances occur for CuLo versus CuLoFeHi (Fig. 4A and C), nonetheless this difference is significant, as is the difference between CuLoFeHi and CuHiFeHi. This analysis also picks up differences between  $M_{\text{meso}}$  and  $G_{\text{meso}}$ . For  $G_{\text{meso}}$  the greatest similarity is consistently for Ctl versus CuLo (Fig. 4B). It is remarkable that the findings in Fig. 4 present such differences, and so consistently (see data in SM, whether OD-normalized or not, two-dimensional trajectory or three-dimensional, including microcystin). Within the consistency, one interesting point of difference that we observed is that for three-dimensional DTW distances, the largest distance observed shifts from Ctl versus CuHiFeHi to CuLoFeHi versus CuHiFeHi for  $M_{\text{meso}}$ , reflecting the largest univariate

distance for microcystin (see SM).

### 3.3. The microcystin-chalkophore link

Consistent with our previous results, we do not find a prominent microcystin-siderophore relationship (see SM). A major motivation for this work, and indeed a major finding of it, concerns the link between microcystin and chalkophore production (Li et al., 2021). The correlation between microcystin and chalkophore is associated with a Spearman's  $\rho$  of 0.68 (Fig. S2) and a Pearson's  $R^2$  of 0.47, in both cases greater than what we previously found for raw results (Fig. S2,  $\rho = 0.53$ , and Fig. 2,  $R^2 = 0.28$  in Li et al., 2021, albeit for selected mesocosms we found  $\rho = 0.77$  and  $R^2 = 0.78$  in Li). Looking only at  $M_{\text{meso}}$  and  $B_{\text{meso}}$  mesocosms (those with *Microcystis*), however, we had found a  $R^2 = 0.61$  at t6 in our previous work for the correlation between microcystin and chalkophore. Clearly, timing should be relevant to the relationship, and of course, we had already anticipated that year-on-year differences would occur. The matter is further complicated by what we now know to be the inherent and likely varying phase-dependencies in the data. Fig. 5 shows results obtained for  $M_{\text{meso}}$  and  $B_{\text{meso}}$  using time-lagged cross correlation, appropriate for phase-linked data, to further examine the microcystin-chalkophore link. The optimum time-lagged Pearson's  $R^2$  is plotted by amendment, as noted on the plots.

As shown in Fig. 5A and B, the time-lagged cross correlations between  $M_{\text{meso}}$  and  $B_{\text{meso}}$  chalkophore and microcystin by amendment are quite strong,  $\sim 0.9$  or above, except for  $M_{\text{meso}}$  CuHiFeHi. The overall correlation between chalkophore and microcystin when combining all data from different amendments is  $R^2 = 0.76$  (Fig. 5C). This is lower than for any of the individual data sets in Fig. 5A–B, but nonetheless, quite a strong correlation.

Aside from the strong correlations, another interesting trend is the progression in slopes, reported in Table 2 below, where we see that values of slope follow the order CuLoFeHi  $\sim$  CuLo  $>$  Ctl  $>$  CuHiFeHi for both  $M_{\text{meso}}$  and  $B_{\text{meso}}$ . For the slopes of the chalkophore-microcystin correlations in Table 2, a higher slope reflects a higher microcystin production for a given increment of chalkophore production (or vice versa). Tukey's HSD was performed to check the differences of those slopes between amendments were significant or not, and the results showed that all the slopes are significantly different ( $p < 0.05$ ) for  $M_{\text{meso}}$  and  $B_{\text{meso}}$  between amendments, except the differences between  $M_{\text{meso}}$  CuLo / CuLoFeHi (where slopes differ by only  $\sim 3\%$ ) and  $M_{\text{meso}}$  Ctl / CuHiFeHi (though with the slope for  $M_{\text{meso}}$  CuHiFeHi being greater than that of  $M_{\text{meso}}$  Ctl by a factor of more than two, and at  $p < 0.26$ , it might not be appropriate to term this as an insignificant difference). That the slope of CuHiFeHi is lowest for both  $M_{\text{meso}}$  and  $B_{\text{meso}}$  is because of

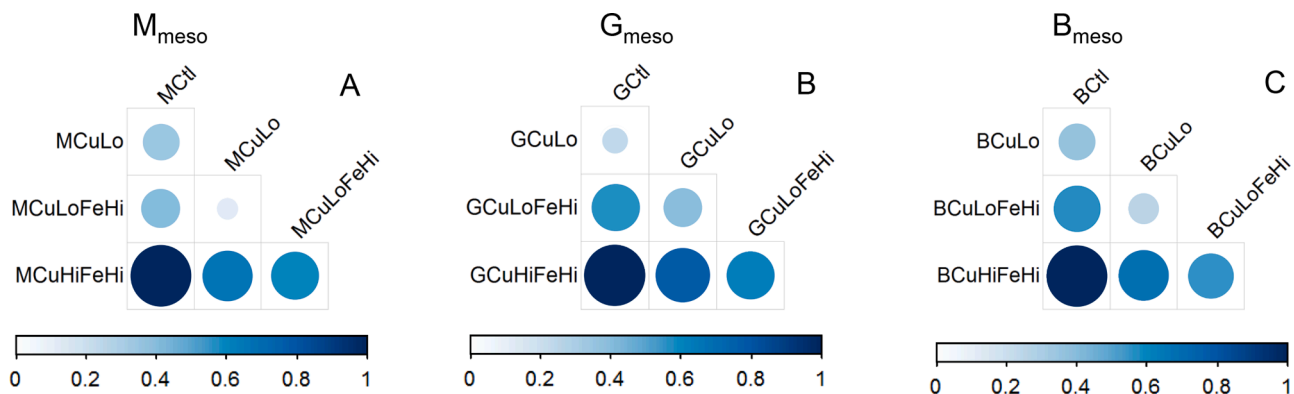


**Fig. 4.** DTW distance matrix plots. Plots show the results of pairwise comparisons for chalkophore/siderophore trajectories. DTW distances within each mesocosm plot ( $M_{\text{meso}}$ ,  $G_{\text{meso}}$ , and  $B_{\text{meso}}$ ) have all been normalized to the maximum. In all cases this is the DTW distance between Ctl and CuHiFeHi, so all distances are normalized to this maximum such that the maximum in the color legend for CuHiFeHi is 1.0 in all cases, and the size and degree of coloration of each circle in the matrix is proportional to the normalized DTW distance. From Tukey's HSD test,  $p$ -values of all pairwise distance comparisons are  $< 0.05$ . (For interpretation of the references to color in this figure legend, the reader is referred to the web version of this article.)



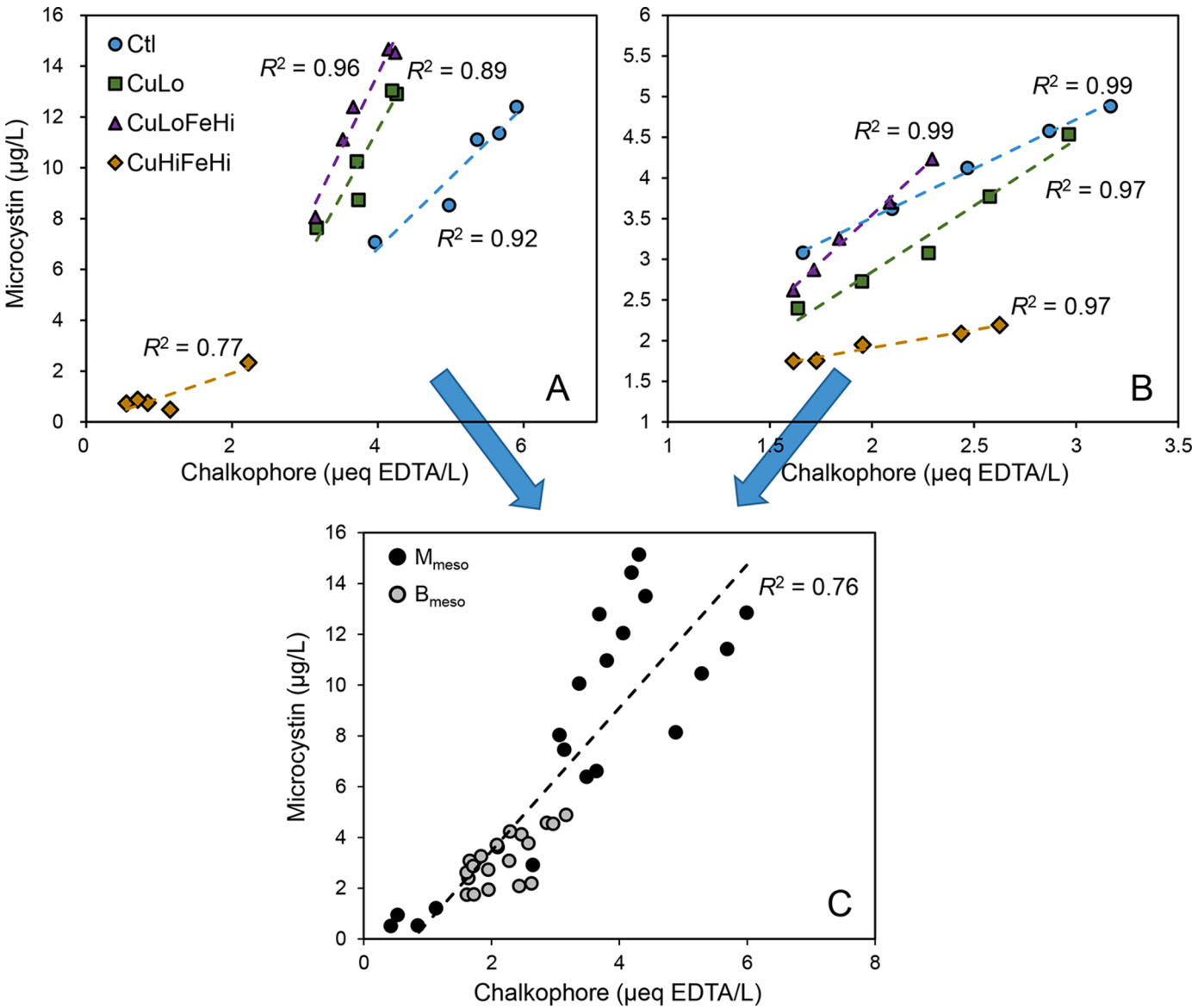


**Fig. 5.** Time-lagged cross correlation for microcystin versus chalkophore. Results are given for (A)  $M_{meso}$ , (B)  $B_{meso}$ , and (C)  $M_{meso}$  and  $B_{meso}$  combined. The dashed lines in panel A and B indicate the trend line for each amendment in the same color as the corresponding symbol (see legend), with  $R^2$  given in black. The dashed line in panel C indicates the trend line for all the data in the panel, with  $R^2$  given in black. (For interpretation of the references to color in this figure legend, the reader is referred to the web version of this article.)

**Table 2**  
Slopes for optimum time-lagged correlation of chalkophore and microcystin.

Mesocosm	Amendments	Slope	Mesocosm	Amendments	Slope
$M_{meso}$	Ctl	2.53	$B_{meso}$	Ctl	1.21
	CuLo	5.42		CuLo	1.63
	CuLoFeHi	5.56		CuLoFeHi	2.32
	CuHiFeHi	1.15		CuHiFeHi	0.44

inhibition of chalkophore production in both cases. For both  $M_{meso}$  and  $B_{meso}$ , when comparing CuLoFeHi with CuHiFeHi, i.e., the amount of Cu is variable, and much more chalkophore relative to microcystin is produced when Cu is low. That the Ctl slope is greater than that for CuLo is suggestive that *Microcystis* increased chalkophore production to capture Cu when the amended Cu is low, but decreased chalkophore production when the amended Cu is too high.

As discussed in Section 2.1, the design of this experiment was, in part, to see if any microcystin-chalkophore link observed is related to Fe

limitation. When comparing the slopes in Table 2, CuLo with CuLoFeHi, where the amount of Fe is variable, the slopes are not differentiable for  $M_{meso}$ . The slopes in Table 2 are significantly different for  $B_{meso}$  CuLo versus CuLoFeHi; however,  $B_{meso}$  slopes have an additional variate: for  $M_{meso}$  and  $B_{meso}$ , respectively,  $m_{M_{meso}} = [\text{Microcystin}, M_{meso}] / ([\text{Chalkophore}, M_{meso}])$ , and  $m_{B_{meso}} = [\text{Microcystin}, M_{meso}] / ([\text{Chalkophore}, M_{meso}] + [\text{Chalkophore}, G_{meso}])$ , where  $m$  is slope,  $[]$  indicates concentration, and it is understood from the data in Fig. 5 that, while  $G_{meso}$  to chalkophore was non-detectable,  $G_{meso}$  (and by extension green algae in  $B_{meso}$ ) started producing chalkophore rapidly.

**3.4. Mechanisms governing the influence of Cu/Fe micronutrients on biomolecule production**

Fig. 6 schematically illustrates selected aspects of Cu/Fe-mediated biomolecule production in  $M_{meso}$  (whereby microcystin production is of particular interest) based on our results and literature results. After algal acclimation to achieve Cu/Fe limitation,  $M_{meso}$  responds to



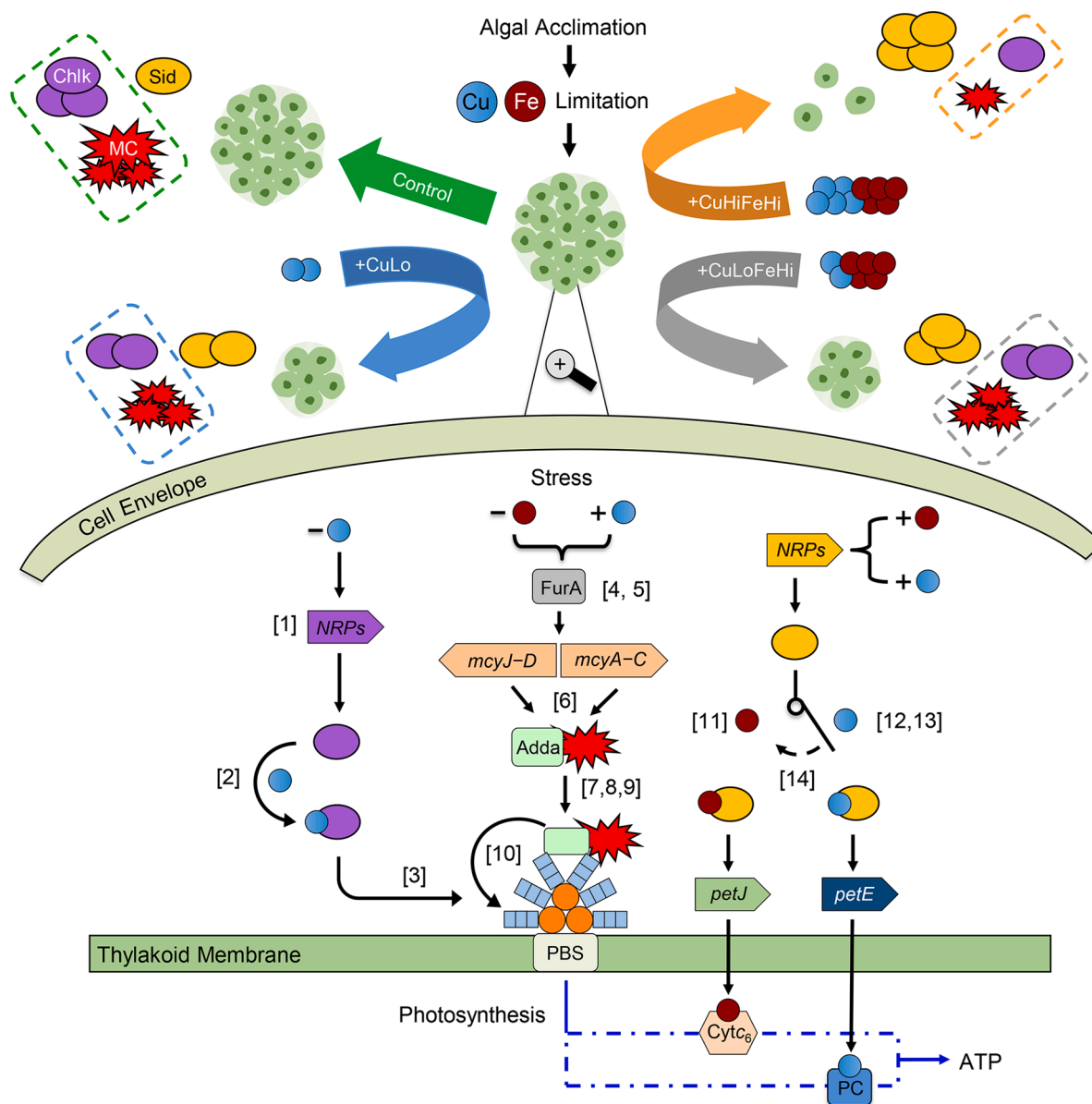


**Fig. 6.** Schematic illustration of biomolecule production in *M<sub>meso</sub>* subsequent to Cu and Fe amendment. The upper part of the schematic illustrates results from our experiments, whereas the lower part of the panel illustrates the crucial roles of Cu and Fe in *Microcystis* spp. photosystems, especially for photosynthetic electron transfer that is involved in the conversion of light energy into ATP production. In the diagram, the biomolecules chalkophore, siderophore, and microcystin are denoted as Chlk, Sid, and MC, respectively; see text for abbreviations and further description of the schematic. Numbers in brackets refer to relevant references for processes shown: [1] Solioz et al., 2018, [2] Kenney and Rosenzweig, 2018, [3] Küpper et al., 2003 [4] Mills and Marletta, 2005, [5] Chen et al. (2020), [6] Tillett et al. (2000), [7] Phelan and Downing, 2014, [8] Fontanillo and Köhn, 2018, [9] Longoni et al., 2019, [10] Derminio, 2020, [11] Saha et al., 2016, [12] Nicolaisen et al., 2010, [13] Hofmann et al., 2020, [14] García-Cañas et al., 2021.

amendments as indicated by the large colored arrows (labelled by amendment: Control, +CuLo, +CuLoFeHi, +CuHiFeHi) at the top of the fig. pointing to graphical depictions summarizing growth and biomolecule production responses (the dashed lines indicate the microcystin-chalkophore links discussed in Section 3.3 above).

At a cellular level, it is reasonable that chalkophore and siderophore, while both binding with very high affinity for their respective cognate metals of Cu and Fe, have nonetheless somewhat different purposes. The behaviour that we observed for *M<sub>meso</sub>* chalkophore in this work is consistent with a circumstance whereby *Microcystis* produces chalkophore through non-ribosomal peptide synthetases (NRPs) in response to lack of Cu (Solioz et al., 2018, bottom left, Fig. 6, also see SM). While siderophores have been reported to be produced via NRPs to capture Fe (Saha et al., 2016), they have also been reported to bind Cu strongly, and

some reports describe an interplay between different types of siderophore production to manage both Cu and Fe (Nicolaisen et al., 2010; Hofmann et al., 2020, see Fig. 6, bottom right), which would be a logical outcome of Cyt<sub>c</sub><sub>6</sub>/PC photosystem's switching. In low Cu conditions, the transcription factor PetR represses the gene *petE* (PC expression) while transcription of the *petJ* gene (Cyt<sub>c</sub><sub>6</sub> expression) is activated by the binding of PetR, such that Cyt<sub>c</sub><sub>6</sub> electron transport dominates. Alternately, in higher Cu conditions, the PetR regulating membrane protease PetP degrades PetR, which results in lower expression of *petJ* and enhanced transcription of *petE*, and thus PC electron transport dominates (García-Cañas et al., 2021). That siderophores bind Cu and Fe, and that *Microcystis* spp. can use either to support photosynthesis, would explain why siderophore production positively correlates with the sum of Cu and Fe amended.

In contrast to chalkophore and siderophore, *why microcystin is produced* is harder to say (bottom center, Fig. 6); it is neither a siderophore, nor a chalkophore (Humble et al., 1997; Yan et al., 2000; Klein et al., 2013), and it is not demonstrated to reduce metal toxicity (Huang et al., 2015; also see SM). From our results and those reported in literature, microcystin production appears to occur at a point where cells are becoming stressed, and there are several diverse known stressors (see SM) that act on the bidirectional *mcy* promoter of the two *mcy* operons (*mcyA–C* and *mcyD–J*, see detailed reported by Tillett et al., 2000). The Fur (ferric uptake regulator) family of regulatory proteins is implicated in the regulation network of several metals (Mills and Marletta, 2005; Porcheron et al., 2013; Kaushik et al., 2016), and specific to this study, FurA, referred to as a “master regulator of Fe homeostasis” (among other functions, Kaushik et al., 2016), can bind to multiple sites of the *mcy* promoter. Both Cu and Fe are known to be associated with FurA stress-associated microcystin production (Martin-Luna et al., 2006b; Chen et al., 2020). The presence of Fe (positive nutritionally, i.e., stress-reducing) has been shown to reduce microcystin production (Martin-Luna et al., 2006b), which is consistent with our results wherein we observe a longer time-lag (1.4 days) for microcystin production in the Fe amendments. In contrast, because Cu is toxic, exposure to high concentrations of Cu is another form of stress, and exposure of *Microcystis* spp. to levels of Cu above that of CuLo in this work has recently been shown to affect microcystin production via the expression of FurA-related genes (Chen et al., 2020, bottom center, Fig. 6).

Some literature implicates microcystin in photosystem function. The Adda (3-amino-9-methoxy-2,6,8-trimethyl-10-phenyl-4,6-decadienoic acid) moiety, produced by the *McyD–J* enzymes (Tillett et al., 2000), is reported to be integral to binding of microcystin to protein phosphatases (Fontanillo and Köhn, 2018). Protein phosphatases have been found to co-localize with phycobilisomes (PBS, i.e. the light harvesting antennae of PSII in cyanobacteria, Longoni et al., 2019), and likewise microcystin has been shown to localize to thylakoid membranes inside cyanobacteria (Phelan and Downing, 2014). These observations taken together imply that microcystin binds to PBS through Adda. Interestingly, recent work by Derminio (2020) suggests that microcystin regulates the movement of the PBS complex and/or changes the arrangement and quantity of phycocyanin (an important pigment-protein complex in the PBS) to prevent excess light energy from entering PSII, thereby decreasing photoinhibition and oxidative stress. Given the intimate connection between Cu/Fe status and photosystem function in *Microcystis* spp., Derminio's findings concerning a microcystin-photosystem link would be consistent with our results here where it appears that microcystin is produced as cells become stressed, by diminution of Cu/Fe availability exacerbated as stationary stage approaches, and need to manage PS productivity to effect an energy-saving status. Photosystem regulation is managed differently by the green algae in  $G_{meso}/B_{meso}$  compared to *Microcystis* spp., in  $M_{meso}$ , and of course since green algae do not produce microcystin, they lack regulatory linkages in biomolecule production that *Microcystis* spp. have. The *CytC6/PC* switching activity is present for some green and other algae (Miramar et al., 2004; Peers and Price, 2006; Merchant et al., 2020), however, expression of the *PC*-encoding gene is constitutive and the regulatory mechanism responsible for switching is not conserved between *PC/CytC6*-expressing green algae and cyanobacteria (Blaby-Haas, 2021). Chalkophore/siderophore responses in  $G_{meso}/B_{meso}$  are discussed briefly in the next section.

The results of this work for  $M_{meso}$  are consistent with multiple lines of evidence from literature for links between nutritional stress conditions involving Cu, Fe, and biomolecule production that in turn affect multiple aspects of photosynthesis and thus energy production of cyanobacteria. Overall, the different micronutrient management needs for Cu (nutrient or toxicant) versus Fe (nutrient) and known cellular mechanisms associated with both suggest that chalkophores are produced as part of a specific cognate response system, whereas the role of siderophores are likely more complex and may involve Cu and Fe. For *Microcystis* spp. this would explain why chalkophore production is more

directly linked with the end-effect of microcystin production than is siderophore, in agreement with our observed  $M_{meso}$  correlations for chalkophore-microcystin. Mathematically speaking, based on the preliminary results in our previous work and results from more detailed study given in Fig. 5, chalkophore is a predictor of microcystin production. More deeply linking molecular results to ecological meaning will no doubt be an interesting area of future research.

### 3.5. Variable trajectories of biomolecule production explained

The trajectories that we report here for biomolecule production are different from those that we previously observed. For  $M_{meso}$ , clockwise trajectories dominate in Fig. 3, however, a counter-clockwise behavior was found for our previous work (Li et al., 2021) comparing Ctl and Fe (200  $\mu\text{g}\cdot\text{L}^{-1}$ ) amended mesocosms. A significant difference between our previous work and the results here is the Cu/Fe limitation status at the onset of mesocosm experiments, which is evident in the t0 levels of TM. In our previous work, t0 TCu and TFe for  $M_{meso}$  were 14 and 400  $\mu\text{g}\cdot\text{L}^{-1}$ , respectively, whereas for this work the levels were 2 and 122  $\mu\text{g}\cdot\text{L}^{-1}$ , respectively. This difference also entails a substantive change in the Fe/Cu ratio. Based on the work of Ji and Sherrell (2008) for *Microcystis* growing in media designed to mimic natural lacustrine/non-depleted conditions, the Fe/Cu ratio is on the order of 10. The t0 Fe/Cu ratio for the *Microcystis* used to dose  $M_{meso}$  in Li et al. (2021) was 29, versus 61 for the work here. Not only is *Microcystis* in  $M_{meso}$  more Cu depleted compared to Fe in both years, but the approach that we took to acclimation for this work to intensify Cu/Fe limitation had an even more pronounced effect on Cu depletion. Though  $M_{meso}$  showed different phasing, the trajectories in Li et al. (2021) versus here are all, as we would describe it, adaptive/rotational when compared to those trajectories for green algae. Trajectories for green algae in Li et al. (2021) are even more heavily siderophore dominated, and for both the present work and that of Li, given the same acclimation procedures, the green algae consistently have more Cu and thus a lower Fe/Cu ratio; while the Fe/Cu  $M_{meso}$  ratio was a factor of two higher here versus Li et al. (2021), the same differential (increased Cu limitation) is only 25% for green algae used in  $G_{meso}$ . Trajectories of  $B_{meso}$  in Fig. 3 are more similar to trajectories of green algae, however, trajectories of  $B_{meso}$  in our previous work were more like  $M_{meso}$ . This is sensible based on the different changes in algal assemblages (green algae-dominated here in  $B_{meso}$  (Fig. 2), BG-dominated in  $B_{meso}$  in our previous work, Li et al., 2021); strikingly, for Li et al. (2021), the  $B_{meso}$  Fe/Cu ratio was 22, which is quite Cu replete compared to 59 for this work. It is a striking result that the failure of *Microcystis* to outcompete green algae in these experiments, compared to Li et al. (2021), is accompanied by such a profound difference in Cu status.

We found that the very different behaviors of *Microcystis* and green algae with respect to chalkophore and siderophore production are very well reflected by the different trajectories. For green algae, it seems indeed that chalkophore production is an ancillary process, with siderophore production being in all cases more prominent. Chalkophore production for *Microcystis* is much more consistent with high cellular Cu requirements here and in our previous work. Based on the interrelationship with siderophore production from *Microcystis*, there does appear to be an active interplay between Cu and Fe management. While the results here concerning the relative timing of chalkophore and siderophore production vary from those in our previous work, the dynamics and magnitude of effects are similar. Our previous results are in keeping with the schematic representation of biomolecules production for *Microcystis* shown in Fig. 6, despite the quite different initial Cu and Fe status of algae from those used in this work.

In addition to different trajectories for chalkophore/siderophore compared to our prior work, differences were also found for the microcystin-chalkophore link. Fig. 7 is a comparison of the microcystin-chalkophore relationships from our previous work and this work. A striking feature in Fig. 7 is that the production of microcystin relative to

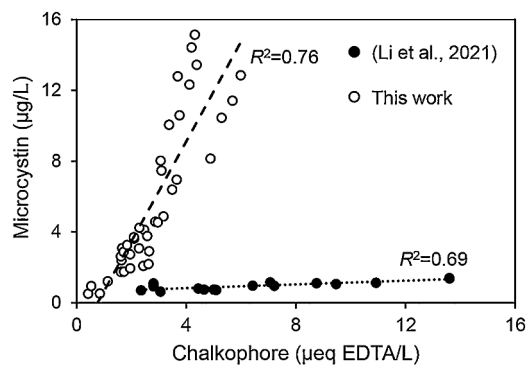


Fig. 7. Microcystin-chalkophore relationships from our previous work and this work. The  $p$ -value  $< 0.001$  in both cases. For both studies we find that the  $R^2$  values are generally higher when assessed for different amendments individually (e.g., compare  $R^2$  values in Fig. 5A and B to Fig. 5C).

chalkophore is much higher in this work as compared to our previous work, (slope for this work is  $\sim 20$  higher than the slope for data from previous work,  $R^2$  as in Fig. 7,  $p < 0.001$ ). The microcystin-to-chalkophore ratio is associated with greater  $t_0$  Cu and Fe limitation (the greater the initial Fe/Cu ratio, the higher the microcystin-to-chalkophore production). This is consistent with the discussion that microcystin is a stress-condition product, here specifically associated with micronutrient stress. The results in Fig. 7 reinforce the finding related to Fig. 5, i.e., chalkophore is a predictor of microcystin production. The governing factors controlling the slope need to be elucidated, however, based on our analysis here, the underlying causative factors relate to both Cu and Fe status. This link between chalkophore production, Cu, and Fe is also clear, as demonstrated by the correlation between chalkophore production and the Cu/Fe ratio for  $M_{\text{meso}}$  in this work (average  $R^2 = 0.83$  for all the time points, with  $p < 0.001$  for each time point, see detailed results in SM).

#### 4. Conclusions

The results presented herein show the following:

- For *Microcystis*/ $M_{\text{meso}}$ , chalkophore production is strongly correlated with Cu, whereas siderophore production for all mesocosms consistently exhibited the strongest correlations with the sum of Cu and Fe.
- *Microcystis* spp. manage Cu/Fe requirements through a dynamically phased behavior of chalkophore/siderophore production that shows significant differences in trajectories according to, and in response to, specific differences in Cu and Fe status and amendment.
- Results suggest that chalkophore production is more prominently active by *Microcystis* spp. compared to the green algae/ $G_{\text{meso}}$ , and that chalkophore production is targeted to cellular cognate recognition mechanisms, whereas mechanisms involving siderophore may also involve Cu.
- We consistently observe a strong microcystin-chalkophore relationship, and chalkophore is a predictor of microcystin production.
- Results here and from prior mesocosm work fit with an emergent body of literature that supports a mechanism wherein *Microcystis* spp. produces microcystin in response to diminution of Cu/Fe availability to manage photosystem productivity and effect an energy-saving status.

Green algae/ $G_{\text{meso}}$ , appear to be able to manage Cu more efficiently than  $M_{\text{meso}}$ /*Microcystis*, and are consequently less impacted by Cu stress. A singular observation reported here for  $B_{\text{meso}}$ /mixed mesocosms is the dramatic difference in the ability of *Microcystis* to hold its own in the presence of green algae in relatively Cu replete conditions, and vice versa. Understanding possible links of Cu-Fe-microcystin is important in

turn to understand how micronutrients might play a role in environmental management, as well as being an exciting new avenue in research to discover the ecological function of microcystin production by *Microcystis* spp.

#### Declaration of Competing Interest

The authors declare that they have no known competing financial interests or personal relationships that could have appeared to influence the work reported in this paper.

#### Data availability

Data will be made available on request.

#### Acknowledgments

This work was supported by the National Natural Science Foundation of China (Grant No. 41571485). We are grateful to Dr. Jianming Deng and the Taihu Laboratory for Lake Ecosystem Research (TLER), Chinese Academy of Sciences, for water quality data and their extensive expertise and assistance with all aspects of work. We also thank Jolien Snellen for help with graphics/figures.

#### Supplementary materials

Supplementary material associated with this article can be found, in the online version, at doi:10.1016/j.watres.2023.120490.

#### References

- Andersen, R.A., 2005. *Algal Culturing Techniques*, first ed. Elsevier/Academic Press, Burlington, Massachusetts.
- Andrei, A., Öztürk, Y., Khalfaoui-Hassani, B., Rauch, J., Marckmann, D., Trasnea, P.I., Daldal, F., Koch, H.G., 2020. Cu homeostasis in bacteria: The ins and outs. *Membranes* 10, 242.
- Badarau, A., Dennison, C., 2011. Thermodynamics of copper and zinc distribution in the cyanobacterium *Synechocystis* PCC 6803. *P. Natl. A. Sci.* 108, 13007–13012.
- Bar-Joseph, Z., Gerber, G.K., Gifford, D.K., Jaakkola, T.S., Simon, I., 2003. Continuous representations of time-series gene expression data. *J. Comput. Biol.* 10, 341–356.
- Bilgrami, K.S., Kumar, S., 1997. Effects of copper, lead and zinc on phytoplankton growth. *Biol. Plant.* 39, 315–317.
- Blaby-Haas, C.E., 2021. Cyanobacteria provide a new paradigm in the regulation of cofactor dependence. *Proc. Natl. Acad. Sci. USA* 118, e2100281118.
- Brooks, B.W., Lazorchak, J.M., Howard, M.D., Johnson, M.V.V., Morton, S.L., Perkins, D.A., Reavie, E.D., Scott, G.I., Smith, S.A., Steevens, J.A., 2016. Are harmful algal blooms becoming the greatest inland water quality threat to public health and aquatic ecosystems? *Environ. Toxicol. Chem.* 35, 6–13.
- Butterwick, C., Heaney, S.I., Talling, J.F., 1982. A comparison of eight methods for estimating the biomass and growth of planktonic algae. *British Phycol. J.* 17, 69–79.
- Chen, Y., Yin, J., Wei, J., Zhang, X., 2020. FurA-dependent microcystin synthesis under copper stress in *Microcystis aeruginosa*. *Microorganisms* 8, 832.
- Cleasby, I.R., Wakefield, E.D., Morrissey, B.J., Bodey, T.W., Votier, S.C., Bearhop, S., Hamer, K.C., 2019. Using time-series similarity measures to compare animal movement trajectories in ecology. *Behav. Ecol. Sociobiol.* 73, 1–19.
- De Cáceres, M., Font, X., Oliva, F., 2010. The management of vegetation classifications with fuzzy clustering. *J. Veg. Sci.* 21, 1138–1151.
- De Cáceres, M., Coll, L., Legendre, P., Allen, R.B., Wiser, S.K., Fortin, M.-J., Condit, R., Hubbell, S., 2019. Trajectory analysis in community ecology. *Ecol. Monogr.* 89, e01350.
- de Leeuw, J., Mair, P., 2009. Multidimensional scaling using majorization: SMACOF in R. *J. Stat. Softw.* 31, 1–30.
- Derminio, D.S., 2020. *Interactions Between Light and Production of Microcystins in the Toxic Cyanobacterium Microcystis*. State University of New York College of Environmental Science and Forestry. Doctoral Dissertation.
- Facey, J.A., Apte, S.C., Mitrovic, S.M., 2019. A review of the effect of trace metals on freshwater cyanobacterial growth and toxin production. *Toxins* 11, 643.
- Fontanillo, M., Köhn, M., 2018. Microcystins: Synthesis and structure-activity relationship studies toward PP1 and PP2A. *Bioorg. Med. Chem.* 6, 1118–1126.
- Frost, P.C., Pearce, N.J.T., Berger, S.A., Gessner, M.O., Makower, A.K., Marzetz, V., Nejtgaard, J.C., Pralle, A., Schällick, S., Wacker, Alexander, W., Nicole, D.W., Xenopoulos, M.A., 2023. Interactive effects of nitrogen and phosphorus on growth and stoichiometry of lake phytoplankton. *Limnol. Oceanogr.* 1–13.



- García-Cañas, R., Giner-Lamia, J., Florencio, F.J., López-Maury, L., 2021. A protease-mediated mechanism regulates the cytochrome c6/plastocyanin switch in *Synechocystis* sp. PCC 6803. *Proc. Natl. Acad. Sci.* 118, e2017898118.
- Gleason, J.R., 1999. An accurate, non-iterative approximation for studentized range quantiles. *Comput. Stat. Data An.* 31, 147–158.
- Gobler, C.J., Burkholder, J.M., Davis, T.W., Harke, M.J., Johengen, T., Stow, C.A., Van de Waal, D.B., 2016. The dual role of nitrogen supply in controlling the growth and toxicity of cyanobacterial blooms. *Harmful Algae* 54, 87–97.
- Gobler, C.J., 2020. Climate change and harmful algal blooms: Insights and perspective. *Harmful Algae* 91, 101731.
- Griffiths, M., Garcin, C., Van Hille, R., Harrison, S., 2011. Interference by pigment in the estimation of microalgal biomass concentration by optical density. *J. Microbiol.* 85, 119–123.
- Harke, M.J., Steffen, M.M., Gobler, C.J., Otten, T.G., Wilhelm, S.W., Wood, S.A., Paerl, H.W., 2016. A review of the global ecology, genomics, and biogeography of the toxic cyanobacterium, *Microcystis* spp. *Harmful Algae* 54, 4–20.
- Ho, K.K., Krogmann, D.W., 1984. Electron donors to P700 in cyanobacteria and algae: An instance of unusual genetic variability. *Biochim. Biophys. Acta* 310–316.
- Hofmann, M., Retamal-Morales, G., Tischler, D., 2020. Metal binding ability of microbial natural metal chelators and potential applications. *Nat. Prod. Rep.* 37, 1262–1283.
- Holden, V.I., Bachman, M.A., 2015. Diverging roles of bacterial siderophores during infection. *Metalomics* 7, 986–995.
- Huang, B., Xu, S., Miao, A.J., Xiao, L., Yang, L.Y., 2015. Cadmium toxicity to *Microcystis aeruginosa* PCC 7806 and its microcystin-lacking mutant. *PLoS One* 10, e0116659.
- Humble, A.V., Gadd, G.M., Codd, G.A., 1997. Binding of copper and zinc to three cyanobacterial microcystins quantified by differential pulse polarography. *Water Res.* 31, 1679–1686.
- Ji, Y., Sherrill, R.M., 2008. Differential effects of phosphorus limitation on cellular metals in *Chlorella* and *Microcystis*. *Limnol. Oceanogr.* 53, 1790–1804.
- Kaushik, M.S., Singh, P., Tiwari, B., Mishra, A.K., 2016. Ferric Uptake Regulator (FUR) protein: properties and implications in cyanobacteria. *Ann. Microbiol.* 66, 61–75.
- Klein, A.R., Baldwin, D.S., Silvester, E., 2013. Proton and iron binding by the cyanobacterial toxin microcystin-LR. *Environ. Sci. Technol.* 47, 5178–5184.
- Kochoni, E., Fortin, C., 2019. Iron modulation of copper uptake and toxicity in a green alga (*Chlamydomonas reinhardtii*). *Environ. Sci. Technol.* 53, 6539–6545.
- Kochoni, E., Doose, C., Gonzalez, P., Fortin, C., 2022. Role of iron in gene expression and in the modulation of copper uptake in a freshwater alga: Insights on Cu and Fe assimilation pathways. *Environ. Pollut.* 305, 119311.
- Kruk, C., Martinez, A., de la Escalera, G.M., Trinchin, R., Manta, G., Segura, A.M., Piccini, C., Brenna, B., Yannicelli, B., Fabiano, G., Calliari, D., 2021. Rapid freshwater discharge on the coastal ocean as a mean of long distance spreading of an unprecedented toxic cyanobacteria bloom. *Sci. Total Environ.* 754, 142362.
- Küpper, H., Šetlik, I., Šetliková, E., Ferimazova, N., Spiller, M., Küpper, F.C., 2003. Copper-induced inhibition of photosynthesis: limiting steps of in vivo copper chlorophyll formation in *Scenedesmus quadricauda*. *Funct. Plant Biol.* 30, 1187–1196.
- Kushkevych, I.V., Beno, Y.J., 2013. Cluster and cross-correlation analysis of some physiological parameters by various *Desulfotomobium* sp. and *Desulfomicrobium* sp. bacterial strains of the human intestine. *SOJ Microbiol. Inf. Dis.* 1, 1–9.
- Lane, D.M., 2015. Online Statbook. [http://onlinestatbook.com/2/calculators/studentized\\_range\\_dist.html](http://onlinestatbook.com/2/calculators/studentized_range_dist.html).
- Li, B., Zhang, X., Deng, J., Cheng, Y., Chen, Z., Qin, B., Tefsen, B., Wells, M., 2021. A new perspective of copper-iron effects on bloom-forming algae in a highly impacted environment. *Water Res.* 195, 116889.
- Longoni, P., Samol, I., Goldschmidt-Clermont, M., 2019. The kinase STATE TRANSITION 8 phosphorylates Light Harvesting Complex II and contributes to light acclimation in *Arabidopsis thaliana*. *Front. Plant Sci.* 10, 1156.
- Manahan, S.E., Smith, M.J., 1973. Copper micronutrient requirement for algae. *Environ. Sci. Technol.* 7, 829–833.
- Martin-Luna, B., Hernandez, J.A., Bes, M.T., Fillat, M.F., Peleato, M.L., 2006a. Identification of a ferric uptake regulator from *Microcystis aeruginosa* PCC7806. *FEMS Microbiol. Lett.* 254, 63–70.
- Martin-Luna, B., Sevilla, E., Hernandez, J.A., Bes, M.T., Fillat, M.F., Peleato, M.L., 2006b. Fur from *Microcystis aeruginosa* binds in vitro promoter regions of the microcystin biosynthesis gene cluster. *Phytochemistry* 67, 876–881.
- Max, K., 2021. caret: Classification and Regression Training. R Package Version 6.0-90. <https://CRAN.R-project.org/package=caret>.
- McCune, B., Grace, J.B., 2002. Analysis of Ecological Communities. MJM Software Design, Gleneden Beach, Oregon, USA.
- McKnight, D.M., Morel, F.M.M., 1980. Copper complexation by siderophores from filamentous blue-green algae. *Limnol. Oceanogr.* 25, 62–71.
- Merchant, S., Bogorad, L., 1986. Regulation by copper of the expression of plastocyanin and cytochrome c552 in *Chlamydomonas reinhardtii*. *Mol. Cell. Biol.* 6, 462–469.
- Merchant, S., 1998. Synthesis of metalloproteins involved in photosynthesis: plastocyanin and cytochromes. In: Rochaix, J.D., Goldschmidt-Clermont, M., Merchant, S. (Eds.), *The Molecular Biology of Chloroplasts and Mitochondria in Chlamydomonas*. Kluwer Academic Publishers, Dordrecht, The Netherlands, pp. 597–611.
- Merchant, S.S., Schmollinger, S., Strenkert, D., Moseley, J.L., Blaby-Haas, C.E., 2020. From economy to luxury: Copper homeostasis in *Chlamydomonas* and other algae. *BBA. Mol. Cell Res.* 1867, 118822.
- Millican, J.S., Back, J.A., McFarland, A.M.S., 2008. Nutrient bioassays of growth parameters for algae in the North Bosque River of Central Texas. *J. Am. Water Resour.* 44, 1219–1230.
- Mills, S.A., Marletta, M.A., 2005. Metal binding characteristics and role of iron oxidation in the ferric uptake regulator from *Escherichia coli*. *Biochemistry* 44, 13553–13559.
- Miramar, M.D., Inda, L.A., Saraiva, L.M., Peleato, M.L., 2004. Plastocyanin/cytochrome c6 interchange in *Scenedesmus vacuolatus*. *J. Plant Physiol.* 60, 1483–1486.
- Nair, A., Juwarkar, A.A., Singh, S.K., 2007. Production and characterization of siderophores and its application in arsenic removal from contaminated soil. *Water Air Soil Poll.* 180, 199–212.
- Nicolaissen, K., Hahn, A., Valdebenito, M., Moslavac, S., Samborski, A., Maldener, I., Wilken, C., Valladares, A., Flores, E., Hantke, K., Schleiff, E., 2010. The interplay between siderophore secretion and coupled iron and copper transport in the heterocyst-forming cyanobacterium *Anabaena* sp. PCC 7120. *BBA Biomembr.* 1798, 2131–2140.
- Omidi, A., Esterhuizen-Londt, M., Pflugmacher, S., 2018. Still challenging: the ecological function of the cyanobacterial toxin microcystin—what we know so far. *Toxin Rev.* 37, 87–105.
- Oppenheim, A.V., Schafer, R.W., Buck, J.R., 1999. Sampling of continuous-time signals. In: Horton, M (Ed.), *Discrete-time Signal Processing*. Prentice Hall, New Jersey.
- Paerl, H.W., Huisman, J., 2008. Blooms like it hot. *Science* 320, 57.
- Paerl, H.W., Xu, H., McCarthy, M.J., Zhu, G., Qin, B., Li, Y., Gardner, W.S., 2011. Controlling harmful cyanobacterial blooms in a hyper-eutrophic lake (Lake Taihu, China): The need for a dual nutrient (N & P) management strategy. *Water Res.* 45, 1973–1983.
- Paerl, H.W., 2018. Mitigating toxic planktonic cyanobacterial blooms in aquatic ecosystems facing increasing anthropogenic and climatic pressures. *Toxins* 10, 76.
- Peers, G., Quesnel, S.A., Price, N.M., 2005. Copper requirements for iron acquisition and growth of coastal and oceanic diatoms. *Limnol. Oceanogr.* 50, 1149–1158.
- Peers, G., Price, N.M., 2006. Copper-containing plastocyanin used for electron transport by an oceanic diatom. *Nature* 441, 341–344.
- Phelan, R.R., Downing, T.G., 2014. The localization of exogenous microcystin LR taken up by a non-microcystin producing cyanobacterium. *Toxicol.* 89, 87–90.
- Porcheron, G., Garénaux, A., Proulx, J., Sabri, M., Dozois, C.M., 2013. Iron, copper, zinc, and manganese transport and regulation in pathogenic Enterobacteria: correlations between strains, site of infection and the relative importance of the different metal transport systems for virulence. *Front. Cell. Infect. Microbiol.* 3, 90.
- Qin, B., Xu, P., Wu, Q., Luo, L., Zhang, Y., 2007. Environmental issues of lake Taihu, China. *Hydrobiologia* 581, 3–14.
- Qin, B., Paerl, H.W., Brookes, J.D., Liu, J., Jeppesen, E., Zhu, G., Zhang, Y., Xu, H., Shi, K., Deng, J., 2019. Why Lake Taihu continues to be plagued with cyanobacterial blooms through 10 years (2007–2017) efforts. *Sci. Bull.* 64, 354–356.
- Quiblier, C., Wood, S., Echenique-Subiabre, I., Heath, M., Villeneuve, A., Humbert, J.-F., 2013. A review of current knowledge on toxic benthic freshwater cyanobacteria—ecology, toxin production and risk management. *Water Res.* 47, 5464–5479.
- Quigg, A., 2008. Trace elements. In: Jørgensen, S.E., Fath, B.D. (Eds.), *Ecological Stoichiometry*. Vol. 5 of Encyclopedia of Ecology. Elsevier, Oxford.
- Quigg, A., 2016. Micronutrients. In: Borowitzka, M.A., Beardall, J., Raven, J.A. (Eds.), *Developments in Applied Phycology*, Vol. 6 of The Physiology of Microalgae. Springer, Switzerland.
- R Core Team, 2021. R: A Language and Environment for Statistical Computing. R Foundation for Statistical Computing, Vienna, Austria. <https://www.R-project.org/>.
- Saha, M., Sarkar, S., Sarkar, B., Sharma, B.K., Bhattacharjee, S., Tribedi, P., 2016. Microbial siderophores and their potential applications: a review. *Environ. Sci. Pollut. Res.* 23, 3984–3999.
- Sandmann, G., Böger, P., 1980. Copper-induced exchange of plastocyanin and cytochrome c-533 in cultures of *Anabaena variabilis* and *Plectonema boryanum*. *Plant Sci. Lett.* 417–424.
- Schoffman, H., Lis, H., Shaked, Y., Keren, N., 2016. Iron–nutrient interactions within phytoplankton. *Front. Plant Sci.* 7, 1223.
- Shapiro, J., 1973. Blue-green algae: Why they become dominant. *Science* 179, 382–384.
- Soliz, M., 2018. Copper and bacteria. Evolution, homeostasis and toxicity. Springer Briefs in Molecular Science Series—Biometals. Springer, Cham, Switzerland.
- Sundarajan, D., 2021. Multirate Digital Signal Processing. Digital Signal Processing. Springer, Cham, Switzerland.
- Tillett, D., Dittmann, E., Erhard, M., Von Döhren, H., Börner, T., Neilan, B.A., 2000. Structural organization of microcystin biosynthesis in *Microcystis aeruginosa* PCC7806: an integrated peptide–polyketide synthetase system. *Chem. Biol.* 7, 753–764.
- Ulrich, A.E., Malley, D.F., Watts, P.D., 2016. Lake Winnipeg Basin: advocacy, challenges and progress for sustainable phosphorus and eutrophication control. *Sci. Total Environ.* 542, 1030–1039.
- Wang, L., Cai, Y., Fang, L., 2009. Pollution in Taihu Lake China: causal chain and policy options analyses. *Front. Earth Sci-PRC.* 3, 437.
- Watson, S.B., Miller, C., Arhonditis, G., Boyer, G.L., Carmichael, W., Charlton, M.N., Confesor, R., Depew, D.C., Höök, T.O., Ludsin, S.A., Matsoff, G., McElmurry, S.P., Murray, M.W., Richards, R.P., Rao, Y.R., Steffen, M.M., Wilhelm, S.W., 2016. The eutrophication of Lake Erie: harmful algal blooms and hypoxia. *Harmful Algae* 56, 44–66.
- Xu, H., Zhu, G., Qin, B., Paerl, H.W., 2013. Growth response of *Microcystis* spp. to iron enrichment in different regions of Lake Taihu, China. *Hydrobiologia* 700, 187–202.
- Xu, H., Paerl, H.W., Zhu, G., Qin, B., Hall, N.S., Zhu, M., 2017. Long-term nutrient trends and harmful cyanobacterial bloom potential in hypertrophic Lake Taihu, China. *Hydrobiologia* 787, 229–242.
- Xue, Q.J., Steinman, A.D., Xie, L.Q., Yao, L., Su, X.M., Cao, Q., Zhao, Y.Y., Cai, Y.J., 2020. Seasonal variation and potential risk assessment of microcystins in the sediments of Lake Taihu, China. *Environ. Pollut.* 259, 113884.
- Yan, F., Ozsoz, M., Sadik, O.A., 2000. Electrochemical and conformational studies of microcystin-LR. *Anal. Chim. Acta* 409, 247–255.



- Yuan, Y., Chen, Y.P.P., Ni, S., Xu, A.G., Tang, L., Vingron, M., Somel, M., Khaitovich, P., 2011. Development and application of a modified dynamic time warping algorithm (DTW-S) to analyses of primate brain expression time series. *BMC Bioinformatics* 12, 1–13.
- Zhang, X., Li, B., Xu, H., Wells, M., Tefsen, B., Qin, B., 2019. Effect of micronutrients on algae in different regions of Taihu, a large, spatially diverse, hypereutrophic lake. *Water Res.* 151, 500–514.
- Zhen, Z.H., Qin, S., Ren, Q.M., Wang, Y., Ma, Y.Y., Wang, Y.C., 2021. Reciprocal Effect of copper and iron regulation on the proteome of *Synechocystis* sp. PCC 6803. *Front. Bioeng. Biotechnol.* 9, 673402.
- Zhou, C., Chen, H., Zhao, H., Wang, Q., 2021. Microcystin biosynthesis and toxic effects. *Algal Res.* 55, 102277.